JOURNAL OF APPLIED ELECTROCHEMISTRY 21 (1991) 991–997

Study of a laboratory filter-press cell by impedance spectroscopy

G. BARRAL, S. MAXIMOVITCH, C. MONTELLA

Ecole Nationale Supérieure d'Electrochimie et d'Electrométallurgie de Grenoble, Centre de Recherche en Electrochimie minérale et en Génie des Procédés, U.A. C.N.R.S. 1212, Domaine Universitaire, B.P. 75, 38402 Saint Martin d'Hères, France

Received 30 October 1990; revised 7 March 1991

Impedance spectroscopy is often used in the laboratory to study the kinetics of electrochemical systems with rotating disc electrode devices. A possible application of this method may be the control of electrochemical processes because it allows analysis of a system over a large frequency range, measurement of reaction or cell parameters like the electrolyte ohmic drop and the interfacial capacitances, and characterization of the kinetics of electron transfer and the hydrodynamic behaviour of the electrolyte. In this work the feasibility of studying the kinetics of an electrochemical system by voltammetry and impedance spectroscopy in a laboratory filter-press cell is described, under conditions approximating those of a subsequent industrial plant. Using a model system such as Fe III complex reduction in an aqueous solution of KOH on a titanium electrode, the hydrodynamics of the cell was studied from the low frequency part of the impedance diagram, corresponding to the diffusion-convection impedance. The results were described as a first approximation by the Nernst model and were consistent with the description of the system under steady-state conditions.

1. Introduction

Impedance spectroscopy is often used to study electrochemical systems to obtain a better understanding of electrochemical reactions such as dissolution or deposition of metals, corrosion or insertion in electrode materials for batteries. More practically, it is also used to measure electrolyte conductivities, determine corrosion rates for metals and alloys and characterize the discharge of batteries, etc [1, 2].

Another possible application of this method is the control of electrochemical processes. For many processes, it is important to measure reaction or cell parameters during operation. In electrochemical engineering, the mass transport coefficient is generally determined by steady-state current measurements with kinetical control by the diffusion of reactive species. Impedance spectroscopy offers extended possibilities: for instance, it allows analysis of a system over the entire frequency range, measurement of the electrolyte ohmic drop and the interfacial capacitances and characterization of the kinetics of electron transfer and the hydrodynamic behaviour of the electrolyte. These impedance measurements are possible over the full potential range and allow the study of mixed conditions of mass transport and electron transfer. It may be expected that impedance measurements carried out on one or both operating electrodes, or on any part of the cell (membrane, for example) and compared with typical diagrams obtained in normal conditions, could act like an electrochemical sensor, allowing the evaluation of the shift from normal behaviour.

Most impedance results have been obtained in the laboratory with rotating disc electrode devices. The aim of this work was to point out the feasibility of conducting impedance measurements with a cell similar to an industrial electrolyser. Impedance measurements were carried out with a simple redox system, first on a rotating disc electrode, then in a laboratory filter-press cell with electrolyte circulation. The chosen reaction was Fe III complex reduction, in an aqueous solution of KOH, on a titanium electrode exhibiting good mechanical properties and electrolyte resistant under the studied conditions.

2. Experimental details

Experiments were carried out at ambient temperature. The electrolyte was an aqueous solution of $K_3[Fe(CN)_6]$ and $K_4[Fe(CN)_6]$, each at a concentration of 5×10^{-2} M, and of KOH 1 M. Measurements at the rotating disc electrode were carried out in an argon atmosphere and in a closed Pyrex cell. The working electrode was the cross section of a titanium round bar, with a geometrical area of 0.196 cm^2, coated with PTFE and fixed on a rotating electrode (Tacussel). The titanium surface was mechanically polished with diamond paste (1 μm), then cleaned in an ultrasonic system and rinsed in alcohol and water before each run. The cell also contained a calomel reference electrode (SCE) and a platinum auxiliary electrode.

The filter-press cell (Fig. 1) was composed of PTFE frames and titanium plates, tightened on silicone rubber gaskets which delimited an active area of 12 cm^2 on the working electrode. The titanium auxili-

0021-891X/91 $03.00 + .12

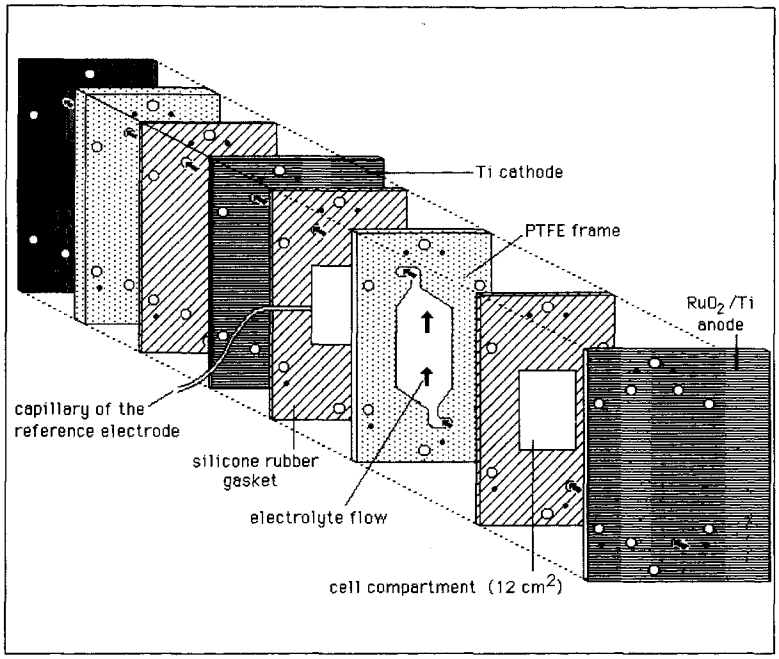

Fig. 1. Schematic representation of the filter-press cell.

ary electrode was covered with ruthenium dioxide. A Luggin capillary, situated in the middle of one side of the electrolysis compartment, joined it to a calomel reference electrode.

The electrolyte circuit was adapted for impedance measurements: a very regular flow was required to limit the scatter of low frequency impedance measurements. The cell was supplied by an overhead reservoir. The flow rate depended on the difference in levels between the reservoir and the cell (2 m) and on the loss of head which depended on the cross section of the pipes (0.34 cm^2) and the cell entrance (0.1 cm^2). The flow rate was measured with a ball flowmeter. In this configuration, the maximum flow rate was 15 $cm^3 s^{-1}$. The compartment was 0.6 cm thick and 3 cm wide, hence the maximum velocity was 8.3 $cm s^{-1}$.

All measurements at the rotating disc electrodes and in the filter-press cell were carried out with three electrodes in potentiostatic mode. For voltammetric measurements, a PRT 20-2X potentiostat (Tacussel) was used. Impedance measurements were conducted with a Schlumberger 1172 frequency response analyser and a 1186 electrochemical interface, and with a 9836 Hewlett Packard computer. Impedances were measured between the working electrode and the reference electrode. Potentials were referred to the saturated calomel electrode (SCE).

3. Measurements with a rotating disc electrode

These measurements were carried out under well defined hydrodynamic conditions and acted as a reference for subsequent studies in the filter-press cell.

3.1. *Voltammograms and steady-state measurements*

Voltammograms were plotted for a potential sweep of 100 $mV s^{-1}$ and various electrode rotation rates, r, in r.p.m. (Fig. 2). The absolute value of the reduction overpotential of Fe III complex was much higher than that measured with, for example, a platinum electrode. It depended on the direction of the potential sweep as may be seen from the hysteresis observed on the curves. Over the entire studied potential range, the titanium electrode is covered with a TiO_2 layer which is an n type semiconductor. The barrier effect related to this type of conduction prevented any oxidation of Fe II complex in the anodic polarization range. At the bottom of the voltammetric wave, the reduction kinetics of Fe III was limited by the electron transfer at the TiO_2 electrolyte interface and the current density did not depend on the rotation rate of the electrode. Then, it was simultaneously limited by the electron transfer and by the transport of Fe III species in the electrolyte, and finally by the transport alone for potential values lower than -1 V. The overpotential depends on the doping level of the semiconducting

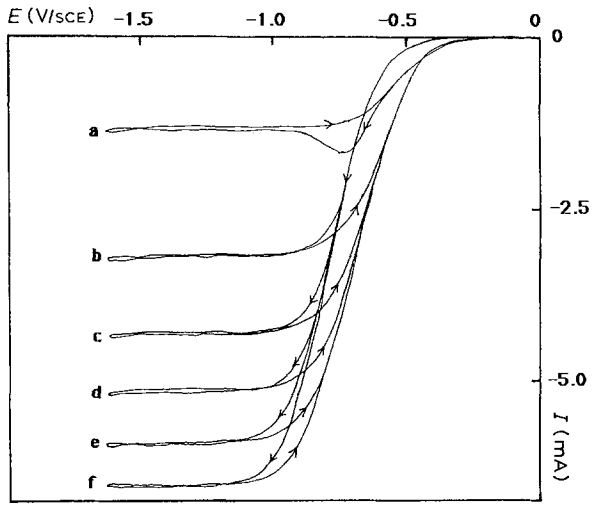

Fig. 2. Measurements with a rotating disc electrode: influence of the electrode rotation rate r on the voltammogram at 100 $mV s^{-1}$; S = 0.196 cm^2. r (r.p.m.) = 0 (a), 500 (b), 1000 (c), 1500 (d), 2000 (e), 2500 (f).

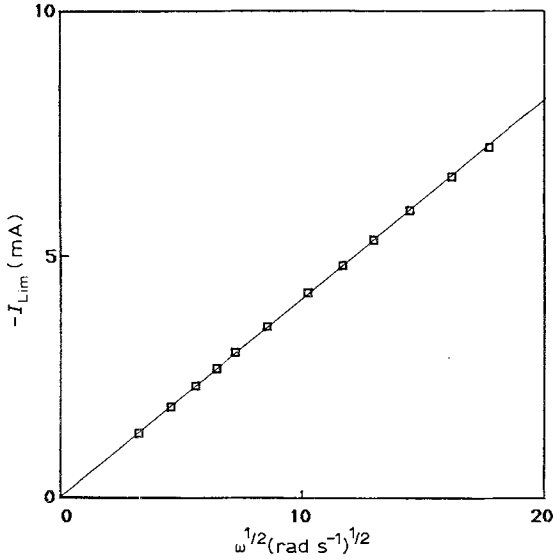

Fig. 3. Measurements with a rotating disc electrode: variation of the steady-state limiting diffusion-convection current with the square root of the rotation rate $\omega = \Pi r/30$.

oxide layer. The hysteresis of the voltammograms may be due to a modification in the doping level of the oxide by an insertion-deinsertion process during the single and return sweep, as recently proposed [3].

The steady-state current density measured on the limiting diffusion-convection plateau followed the Levich law. The diffusion coefficient of Fe III complex was calculated from the slope of the I_{lim} against $\omega^{1/2}$ straight line in Fig. 3, where ω is the electrode rotation rate in rad s^{-1}, assuming the active electrode area equal to the geometrical area and taking $\nu = 1.064 \times 10^{-2}$ cm^2 s^{-1} [4] for the kinematic viscosity of the solution. Therefore

$$D_{Fe\,III} = 5.8 \times 10^{-6}\ \text{cm}^2\ \text{s}^{-1}$$

This value is in good agreement with results found in the literature. Using it, a Schmidt number of $Sc = \nu/D = 1830$ was calculated.

3.2. *Impedance measurements*

Impedances were measured for several electrode potentials and were plotted in the electrochemists' Nyquist plane (Re Z, $-$Im Z). For low current densities (Fig. 4a), a semi-circle appeared at high frequencies, which may be modelled by the parallel connection of the transfer resistance R_t and the interface capacitance C_i. The frequency measured at the top of the semi-circle followed the relation $2\pi f_i R_t C_i = 1$ and characterized, for a given potential, the interface state (C_i) and the kinetics of electron transfer (R_t). The interface capacitance, C_i, was the series connection of the charge space capacitance of the semiconducting TiO_2 layer and of the double layer capacitance of the electrolyte, C_{dc}. The C_i value, lower than that measured on a metal where $C_i = C_{dc}$ was, however, of the same order. On the other hand, the value of the transfer resistance related to the doping level of the TiO_2 layer was higher than for a metal such as platinum. This explained why the high frequency arc was observed in the frequency measurement range ($f < 10^4$ Hz) whereas it cannot be seen for a platinum electrode.

The diffusion-convection impedance of Fe III species appeared in the low frequency range. Its relative importance increased as the current density increased (Fig. 4b and c). Close to 10 Hz, a linear part making a 45° angle with the real axis, characteristic of the Warburg impedance, was observed. When the diffusion-convection plateau was reached, the transfer resistance became negligible (Fig. 4d).

The influence of electrode rotation rate was studied at an electrode potential of -0.85 V where the two impedance arcs are well separated and the imaginary part of the impedance was plotted versus the logarithm of frequency for several electrode rotation rates (Fig. 5). As the rotation rate increased, the relative extent of the diffusion impedance increased and the characteristic frequency, f_c, at the extremum of $-$Im Z is the low frequency range shifted towards low frequencies. The value of f_d was determined by parabolic approximation around the extremum.

With the Nernst approximation of the concentration profile near the disc electrode, f_d is theoretically expressed as [5–8]

$$2\pi f_d = 2.53 D/\delta^2 \qquad (1)$$

The constant in Equation 1 varies from 2.52 to 2.54 depending on the authors. D is the diffusion coefficient of the electroactive species and δ is given by Levich theory [9]

$$\delta = 1.61 D^{1/3} \nu^{1/6} \omega^{-1/2} \qquad (2)$$

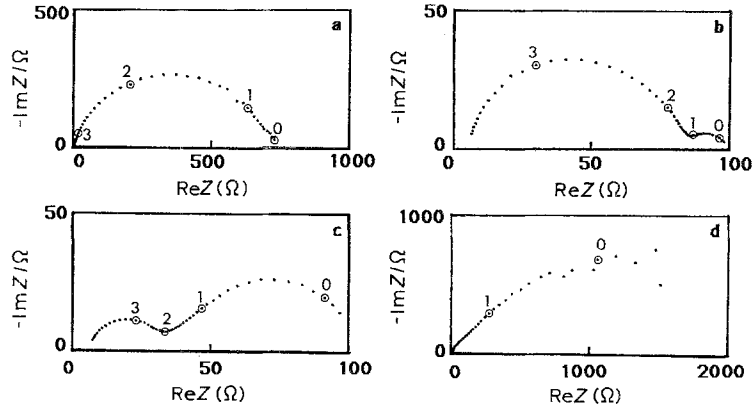

Fig. 4. Measurements with a rotating disc electrode: influence of the electrode potential on the impedance diagram. $r = 2000$ r.p.m. Potential: (V/SCE) $= -0.5$ (a) -0.7 (b), -0.9 (c), -1.1 (d). Parameters: logarithm of frequency (Hz).

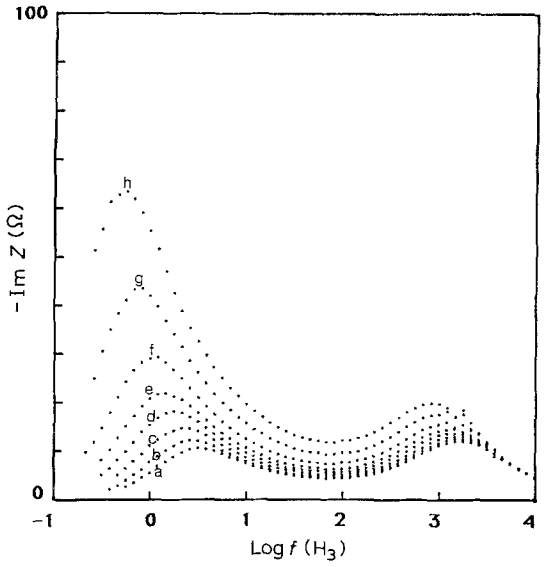

Fig. 5. Measurements with a rotating disc electrode: variation of the imaginary part of the impedance with the logarithm of frequency for several rotation rates, at the potential of −0.85 V/SCE. r (r.p.m.) = 3000 (a), 2500 (b) 2000 (c), 1600 (d), 1300 (e), 1000 (f), 700 (g), 500 (h).

So, f_d varies linearly with ω

$$2\pi f_d = 0.98(D/\nu)^{1/3}\omega = 0.98Sc^{-1/3}\omega \quad (3)$$

where Sc is the Schmidt number already mentioned.

Taking into account a more realistic profile of concentration near the disc, Levart and Schuhmann solved the diffusion-convection equation using a series expansion [10]. They defined a dimensionless frequency, $u = (2\pi f/\omega)Sc^{1/3}(0.510)^{-2/3}$ and tabulated the real and imaginary parts of the impedance as a function of u for $Sc = \infty$, $Sc = 10^3$ and $Sc = 10^2$. They also gave correction parameters which allowed calculation of the impedance for intermediate values of Sc. By polynomial interpolation of these tabulated impedance data, we numerically determined the characteristic frequency $u_d = (2\pi f_d/\omega)Sc^{1/3}(0.510)^{-2/3}$ which dependend on Sc, in opposition to the Nernst model (Equation 3).

In the range $1000 < Sc < 2000$, u_d could be approximated by $u_d = 1.22 + 2 \times 10^{-5} Sc$. Then

$$2\pi f_d = 0.638Sc^{-1/3}(1.22 + 2 \times 10^{-5} Sc)\omega$$
$$\text{for } 1000 < Sc < 2000 \quad (4)$$

The variation of f_d with the rotation rate ω is represented in Fig. 6a. The Sc values were determined from the slope of the straight line using Equation 4, then the diffusion coefficient was calculated as $D = \nu/Sc$:

$$Sc = 1797 \text{ and } D_{Fe^{III}} = 5.9 \times 10^{-6} \text{ cm}^2 \text{ s}^{-1}$$

This method of determination of the diffusion coefficient is independent of the species concentration and of the real area of the electrode, as opposed to the method based on the steady state I_{lim} against $\omega^{1/2}$ relation. However, because the values of f_d appeared in the low frequency range, the effect of the relative imprecision of $\Delta f_d/f_d$ on the determination of f_d and then on the slope was not negligible. It followed an inaccuracy in the determination of $D_{Fe^{III}}$, because the slope of the straight line of Fig. 6a was raised to a power of 3 to estimate Sc from Equation 4. In view of the inaccuracy of impedance data and of limiting steady-state currents, the values of $D_{Fe^{III}}$ obtained by these two methods were consistent. In Fig. 6a the f_d values calculated using the Nernst approximation from Equation 3 are also reported as the dashed line. In Fig. 6b, the results are plotted using a bi-logarithmic scale. It may be seen that the Nernst model, despite its approximate character, provides a first approximation of the diffusion-convection model at a rotating disc electrode.

4. Filter-press cell measurements

The presence of a reference electrode in the filter-press cell (Fig. 1) allowed measurement of electrochemical kinetics as with a classical electrolysis cell.

4.1. *Voltammograms and steady state measurements*

Voltammograms were obtained for a potential sweep of 100 mV s^{-1} and for several values of the electrolyte flow rate (Fig. 7) and the steady-state limiting current I_{lim} was measured versus the flow rate at a potential of −1.25 V. These values were plotted versus the velocity of the electrolyte, v_0, using a bilogarithmic scale (Fig. 8a) and in a dimensionless form (Fig. 8b).

The classical correlations found in the literature concerning mass transport express the Sherwood number ($Sh = d/\delta_{av}$) against the Schmidt ($Sc = \nu/D$) and Reynolds ($Re = v_0 d/\nu$) numbers:

$$Sh = kSc^{\alpha}Re^{\beta} \quad (5)$$

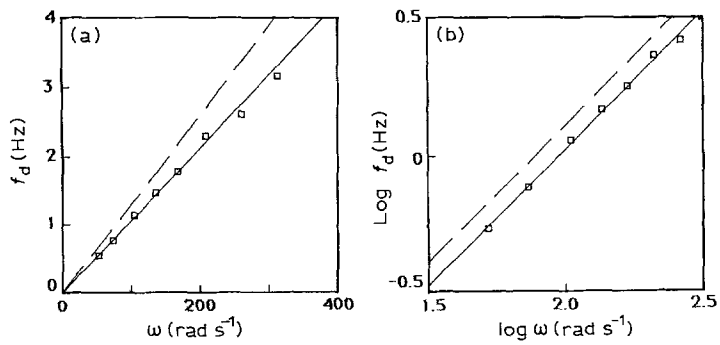

Fig. 6. Measurements with a rotating disc electrode: variation of the characteristic frequency of the diffusion-convection impedance with the rotation rate of the electrode. (a) linear scales, (b) logarithmic scales. (□) Experimental points, (——) Relation 4, (– – –) Relation 3.

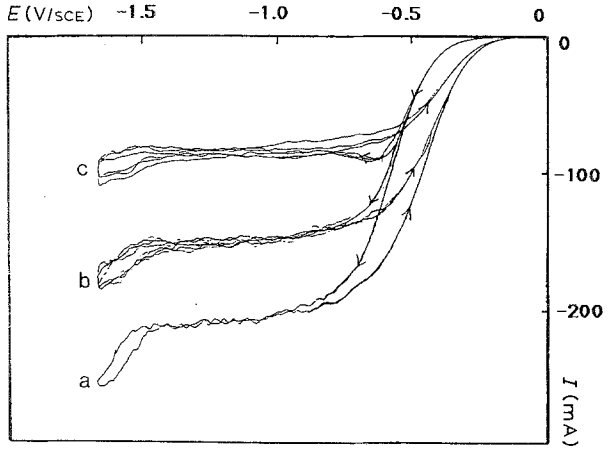

Fig. 7. Measurements carried out in the filter-press: influence of the electrolyte velocity on the voltammogram. $v = 100\,\text{mV s}^{-1}$; $S = 12\,\text{cm}^2$; $v_0\,(\text{cm s}^{-1}) = 7.92$ (a), 3.96 (b), 1.98 (c).

where d is a characteristic length for the cell and δ_{av} is the average thickness of the diffusion layer in the Nernst model

$$\delta_{av} = FSD_{\text{Fe III}}\text{Fe III}^*/I_{lim} \quad (6)$$

Fe III* refers to the bulk concentration of Fe III complex and S to the electrode area.

In the majority of cases, $\alpha = 1/3$ whereas β depends on the type of hydrodynamic flow (laminar or turbulent) and on the cell geometry.

The cell was assumed to be a rectangular channel with width b and thickness h. The principal correlations found in the literature [11, 12, 13] for this geometry are summarized in Table 1. The average Reynolds number was calculated by assuming that the charactistic length was the hydraulic diameter, d, defined in Table 1 ($d = 1\,\text{cm}$ for the used cell). The maximum linear velocity was $v_0 = 8.33\,\text{cm s}^{-1}$, that is $Re = 783$. These conditions corresponded theoretically to laminar ($Re < 2000$) nondeveloped flow ($l_v = 9.5\,\text{cm}$ for $d = 1\,\text{cm}$) (Table 1).

For the mass transport at the entrance of a channel in nondeveloped laminar flow a variation of Sh with $Re^{0.5}$ may be observed (Table 1), that is a variation of the current with $v_0^{0.5}$. From the slope of the logarithmic plot in Fig. 8a and Fig. 8b, we deduced $\beta = 0.71$. This high exponent is characteristic of turbulent flow or for the transition range between laminar and turbulent flow (Table 1). The experimental relation describing the mass transport in the filter-press cell did not correspond to a simple theoretical model. Several phenomena may contribute to the turbulent flow: the measured behaviour was the average behaviour over the entire area including the edge effects, which are important due to the small size of the cell. To obtain the laminar flow law, the fluid velocity must be uniform throughout the cell entrance. The channel geometry and the high Reynolds number at this location (narrow opening), led to turbulence which may have modified the subsequent flow. These equations are valid for a smooth surface, however the electrode had some roughness (1 μm), which was of the same order as the thickness of the average diffusion layer on the electrode.

4.2. *Impedance measurements*

4.2.1. General characteristics of the diagrams. The impedance diagrams were plotted for several electrode potentials and for an electrolyte velocity of $7.9\,\text{cm s}^{-1}$. Their general shape was the same as for a rotating disc electrode. At $-0.5\,\text{V}$ (Fig. 9a) the diagram was composed of a single arc corresponding to the transfer resistance in parallel with the interface capacitance. From -0.7 to $-0.8\,\text{V}$ (Fig. 9b and c), it had two parts separated to an extent depending on the electrode potential: the high frequency part was a semi-circle and the low frequency diffusion-convection impedance had a shape analogous to that already measured with the rotating disc electrode (the part which makes a 45° angle with the real axis). At $-1\,\text{V}$, only the diffusion-convection impedance was observed (Fig. 9d).

The influence of cell geometry on different parameters was indicated by the comparison of the diagrams plotted for the two electrolysis cells. The high frequency limit of the impedance diagrams, which represents the sum of the circuit resistances (electrolyte, electrode, contacts), was of the order of $5\,\Omega$ with the rotating disc electrode where there are high contact resistances, and around $0.5\,\Omega$ in the filter-press cell. In the latter case, it may be considered as the resistance of the volume of electrolyte situated between the tip of reference electrode and working electrode,

Table 1. Theoretical correlations for mass transport in a rectangular channel with width b, height h and length l, from [11, 12, 13]

	Hydraulic diameter	$d = 4bh/2(b + h)$
	Developing length	$l_v/d = 0.00648\,Re$
	$Re = v_0 d/\nu$	
Laminar flow	Undeveloped flow	$Sh_{av} = 0.678\,Re_l^{1/2}Sc^{1/3}$
		$Sh_l = k_d l/\nu$ and $Re_l = v_0 l/\nu$
	Developed flow	$Sh_{av} = 1.85[Re\,Sc\,d/l]^{1/3}$
		$Sh = k_0 d/\nu$ and $Re = v_0 d/\nu$
Turbulent flow	Entrance region	$Sh_{av} = 0.276\,(Re)^{0.58}(Sc)^{1/3}(d/l)^{1/3}$
		$Sh = k_0 d/\nu$ and $Re = v_0 d/\nu$
	Developed flow	$Sh_{av} = 0.023\,Re^{0.8}Sc^{1/3}$
		$Sh_{av} = k_0 d/\nu$ and $Re = v_0 d/\nu$

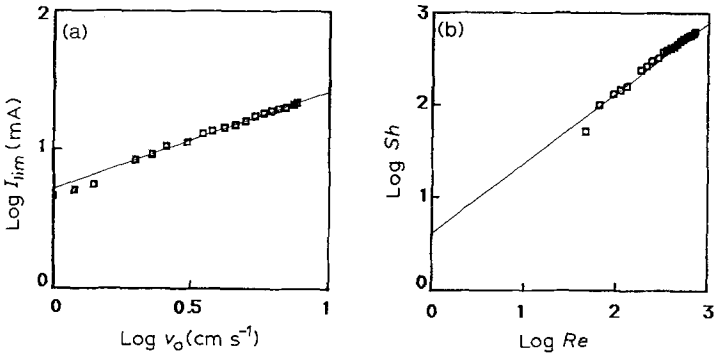

Fig. 8. Measurements carried out in the filter-press cell: variation of the limiting diffusion-convection steady-state current with the electrolyte velocity v_0. (a) log I_{lim} against log v_0; (b) log Sh against log Re.

which is proportional to the thickness of the compartment and inversely proportional to the electrode area. The electron transfer resistance, R_t, and polarization resistance, $R_p = \lim_{f\to 0} Z$, are inversely proportional to the electrode area but their specific values expressed in $\Omega\,cm^2$ are independent of the cell used. At -0.7 V, for example, R_t was 1.5 Ω for the filter-press cell and 90 Ω for the rotating disc electrode and the specific value was 7.5 $\Omega\,cm^2$ for both cells. The high frequency capacitance which characterizes the electrode-solution interface is proportional to the area. Its specific value expressed in F/cm^{-2} was identical for both electrodes (9.2×10^{-6} F cm^{-2}). The characteristic frequency, f_i, measured at the top of the high frequency arc such that $2\pi f_i R_t C_i = 1$, was thus invariable and independent of the electrode size, and characteristic of the activation kinetics, R_t, and of the nature of the interface, C_i. This comparison showed the validity of kinetic measurements carried out in the filter-press cell.

4.2.2. Influence of the electrolyte flow rate. The impedance diagrams were plotted at an electrode potential of -0.7 V where the two arcs of the diagram are well separated and for an electrolyte flow rate varying from 1.42 cm^3 s^{-1} to 13.7 cm^3 s^{-1}, that is a velocity varying from 0.79 cm s^{-1} to 7.6 cm s^{-1} (Fig. 10).

As for the rotating disc electrode, the relative extent of the diffusion-convection impedance varied with the electrolyte flow rate and its shape remained the same. As the flow rate decreased, the characteristic frequency, f_d, measured at the extremum of $-\mathrm{Im}\,Z$ in the low frequency range, moved towards the low frequencies. The bi-logarithmic plot of Fig. 11 shows that f_d varied proportionally to $v_0^{1/4}$.

4.2.3. Interpretation. The theoretical calculation of the convective-diffusion impedance requires knowledge of the concentration profile near the electrode-electrolyte interface, which depends on the electrolyte flow rate given by the solution of the Navier-Stokes equation. Compton and Seally [14] rigorously solved this equation for the case of a fully developed laminar flow. However, the theoretical results of these authors do not apply to our results as we have already pointed out for our steady-state measurements.

Thus, we used the Nernst model approximation which assumes a motionless layer at the interface, in which mass transport takes place only by diffusion. Beyond this layer, the solution is assumed perfectly mixed and the concentrations of the electroactive species are those of the bulk. The impedance was calculated by assuming that the disturbance did not extend beyond the layer δ_{av}. In the filter-press cell, the current density was not uniform at the electrode surface (edge effects) and δ_{av} was regarded as the average thickness of the diffusion layer.

δ_{av} was calculated from I_{lim} data and Relation 6, and substituted in Relation 1. The corresponding values of the calculated characteristic frequency were plotted in Fig. 11. There was therefore a slight difference between the experimental values of f_d measured at the extremum of the diffusion-convection impedance arc and those calculated in the Nernst model from I_{lim}, as was already observed on the rotating disc electrode in Fig. 6a. This is because the Nernst approximation of the concentration near the electrode surface is very crude.

Figure 11 shows that f_d varies with the electrolyte velocity in the filter-press cell as: $f_d = kv_0^{1.4}$. The exponent was in agreement with the steady state

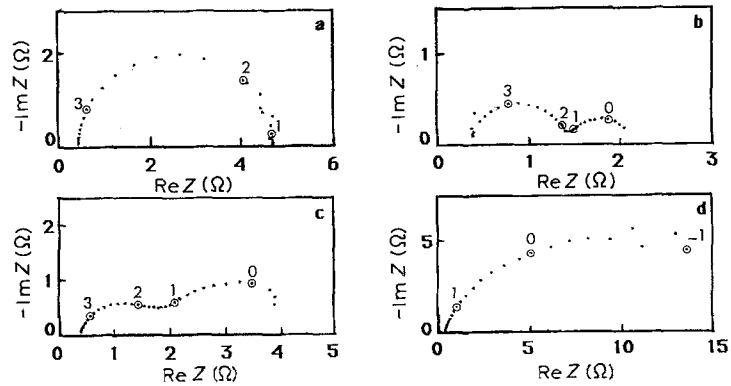

Fig. 9. Measurements carried out in the filter-press cell: influence of the electrode potential on the impedance diagram for an electrolyte velocity of 7.92 cm s^{-1}. Potential: (V/SCE) = -0.5 (a), -0.7 (b), -0.8 (c), -1.0 (d). Parameter: logarithm of frequency (Hz).

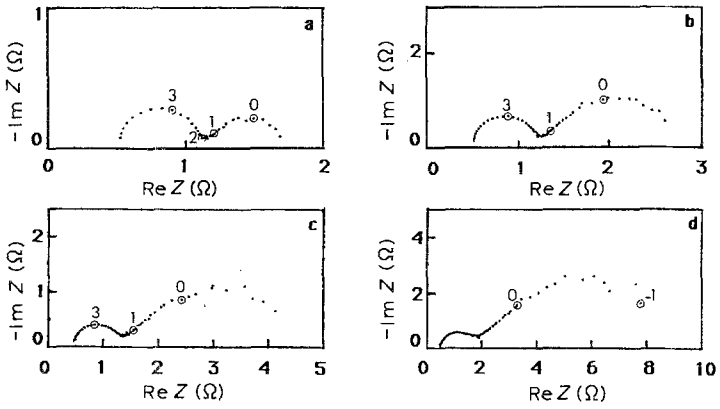

Fig. 10. Measurements carried out in the filter-press cell: influence of the electrolyte velocity on the impedance diagram, at a potential of -0.7 V/SCE. v_0 (cm s^{-1}) = 7.92 (a), 4.95 (b), 3.65 (c), 2.22 (d). Parameter: logarithm of frequency (Hz).

measurements and was characteristic of a turbulent flow or for the transition between a laminar and turbulent flow and the constant k was characteristic of hydrodynamic conditions in the filter-press cell. Its value could be approximated using the Nernst model.

5. Conclusion

Using a model system, such as the reduction of Fe III complex, the possibility of studying the hydrodynamics of an electrolysis cell by impedance spectroscopy was illustrated. The low frequency part of the impedance diagram, corresponding to the diffusion-convection impedance, were described to a first approximation by the Nernst model and the results were consistent with the description of the system under steady-state conditions.

These measurements showed the possibility of studying the kinetics of an electrochemical system by voltammetry and impedance spectroscopy in a mini-pilot filter-press cell and under conditions near those of a subsequent industrial plant.

Impedance spectroscopy allows measurement of characteristics of the cell or the electrode, of electrochemical reaction and the hydrodynamics during operation and over the entire range of frequencies and electrode potentials. This method may find applications to control and eventually optimize the operation of an electrochemical reactor.

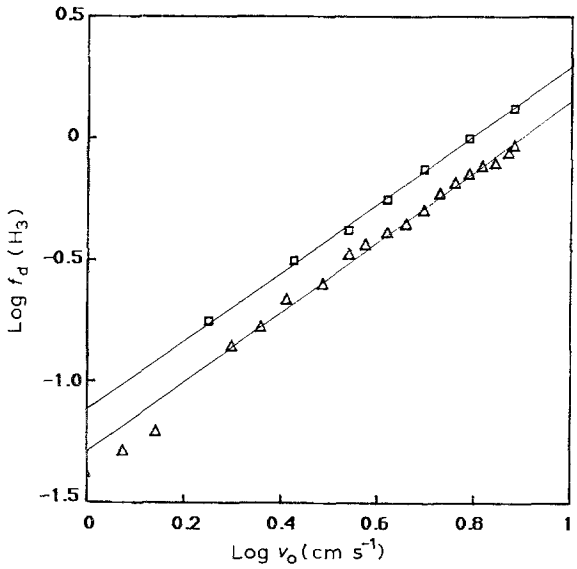

Fig. 11. Bilogarithmic representation of the characteristic frequency of the diffusion-convection impedance versus the electrolyte velocity at a potential of -0.7 V/SCE. (□) Experimental values measured on the impedance diagrams; (△) values calculated with the Nernst model from I_{lim}.

References

[1] M. Sluyters-Rehbach and J. H. Sluyters, 'Electroanalytical Chemistry', Vol. 4, Marcel Dekker, New York (1978).
[2] C. Gabrielli, 'Identification of Electrochemical Processes by Frequency Response', Analysis Solartron Instrumentation Group, Farnborough, UK (1980).
[3] G. Barral and F. Cardot, 'Journees d'Electrochimie', Dijon, France (1987).
[4] 'Handbook of Chemistry and Physics', 61st edition, CRC Press, Boca Ratou, FA USA (1980–1981) D 253.
[5] C. Deslouis, J. Epelboin, M. Keddam and J. C. Lestrade, *J. Electroanal. Chem.* **28** (1970) 57.
[6] J. Bressan and R. Wiart, *J. Appl. Electrochem.* **9** (1979) 615.
[7] J. L. Dawson and D. G. John, *J. Electroanal. Chem.* **110** (1980) 37.
[8] J. P. Diard, B. Le Gorrec, C. Montella and E. Saint Aman, *Electrochim. Acta* **27** (1982) 1055.
[9] V. G. Levich, 'Physiochemical Hydrodynamics', Prentice-Hall, Englewood Cliffs, NJ (1962).
[10] E. Levart and D. Schuhmann, *J. Electroanal. Chem.* **28** (1970) 45.
[11] F. Coeuret and A. Storck, 'Eléments de Génie Electrochimique', Tec-Doc, Lavoisier, Paris (1984).
[12] N. Ibl and O. Dossenbach, 'Convective mass transport, Comprehensive Treatise of Electrochemistry', Vol. 6 (edited by E. Yeager, J. O'M. Bockris, B. E. Conway and S. Sarangapani), Plenum Press, New York (1983).
[13] D. J. Pickett, 'Electrochemical Reactor Design', Elsevier, Amsterdam (1979).
[14] R. G. Compton and G. R. Sealy, *J. Electroanal. Chem.* **145** (1983) 35.